Published in final edited form as:

Int J Cancer. 2020 November 15; 147(10): 2811–2823. doi:10.1002/ijc.33046.

Histone deacetylase inhibition prevents the growth of primary and metastatic osteosarcoma

Jeremy J. McGuire[1,2], **Niveditha Nerlakanti**[1,2], **Chen Hao Lo**[1,2], **Marilena Tauro**[2], **Thomas J. Utset-Ward**[3,4], **Damon R. Reed**[5], **Conor C. Lynch**[2]

[1]Cancer Biology Ph.D. Program, University of South Florida, Tampa, Florida

[2]Tumor Biology Department, H. Lee Moffitt Cancer Center and Research Institute, Tampa, Florida

[3]Department of Drug Discovery, H. Lee Moffitt Cancer Center and Research Institute, Tampa, Florida

[4]Department of Orthopaedic Surgery and Rehabilitation Medicine, University of Chicago, Chicago, Illinois

[5]Sarcoma Department & Department of Interdisciplinary Cancer Management (DICaM), H. Lee Moffitt Cancer Center and Research Institute, Tampa, Florida

Abstract

Overall survival rates for patients with advanced osteosarcoma have remained static for over three decades. An in vitro analysis of osteosarcoma cell lines for sensitivity to an array of approved cancer therapies revealed that panobinostat, a broad spectrum histone deacetalyase (HDAC) inhibitor, is highly effective at triggering osteosarcoma cell death. Using in vivo models of orthotopic and metastatic osteosarcoma, here we report that panobinostat impairs the growth of primary osteosarcoma in bone and spontaneous metastasis to the lung, the most common site of metastasis for this disease. Further, pretreatment of mice with panobinostat prior to tail vein inoculation of osteosarcoma prevents the seeding and growth of lung metastases. Additionally, panobinostat impaired the growth of established lung metastases and improved overall survival, and these effects were also manifest in the lung metastatic SAOS2-LM7 model. Mechanistically, the efficacy of panobinostat was linked to high expression of HDAC1 and HDAC2 in osteosarcoma, and silencing of HDAC1 and 2 greatly reduced osteosarcoma growth in vitro. In accordance with these findings, treatment with the HDAC1/2 selective inhibitor romidepsin compromised the growth of osteosarcoma in vitro and in vivo. Analysis of patient-derived xenograft osteosarcoma cell lines further demonstrated the sensitivity of the disease to

Correspondence: Conor C. Lynch, Department of Tumor Biology, H. Lee Moffitt Cancer Center and Research Institute, 12902, Magnolia Drive, Tampa, FL 33612. conor.lynch@moffitt.org.

CONFLICT OF INTEREST

D. R. is on the Advisory Board for Epizyme. His role is unrelated to work presented in this manuscript. The remaining authors declare no conflict of interest.

DATA ACCESSIBILITY

All data and detailed methods will be made available upon reasonable request.

SUPPORTING INFORMATION

Additional supporting information may be found online in the Supporting Information section at the end of this article.

panobinostat or romidepsin. Collectively, these studies provide rationale for clinical trials in osteosarcoma patients using the approved therapies panobinostat or romidepsin.

Keywords

histone deacetylase; lung metastasis; osteosarcoma; panobinostat

1 INTRODUCTION

Despite being the most prevalent primary bone cancer, the treatment paradigm for osteosarcoma, consisting of high-dose methotrexate, doxorubicin and cisplatin, has changed little over the past three decades.[1,2] Metastasis is the cause of osteosarcoma related deaths, with the lungs being the most prevalent site,[3] and tragically, the 5-year event-free survival for patients with lung involvement is only 28%.[4] Among the provocative questions created by the osteosarcoma biology committee were an improved understanding of metastasis and alterations in copy number, aneuploidy and epigenetic control of osteosarcoma pathogenesis.[5] Due to the rarity of the disease, clinical trials are difficult and time consuming to conduct, underscoring the need for strong preclinical data to inform human trial design. To this end, we assessed the efficacy of approved single agents and combinations using five common human osteosarcoma cell lines, paying particular attention to reported tolerability in clinical trials, nonoverlapping toxicities, pharmacokinetic data, cytochrome P450 metabolism and other characteristics that negate drug-drug interactions.[6] Our in vitro data consistently indicated that the broad spectrum histone deacetylase (HDAC) inhibitor, panobinostat, was cytotoxic for osteosarcoma cells at very low nanomolar concentrations, a finding supported by independent studies.[6]

Panobinostat inhibits all classes of HDACs with varying potency and is currently approved for use in multiple myeloma patients with clinical trials ongoing in other malignancies.[7] The primary mechanism of action of panobinostat is disrupting epigenetic control of transcriptional programs that govern cell growth and survival.[8] However, independent of epigenetic regulation, HDACs can also regulate the activity of several proteins involved in the cell cycle, the production of reactive oxygen species, apoptosis, immune surveillance, angiogenesis and tumor metastasis.[9]

In vitro studies in osteosarcoma cell lines have shown that HDAC inhibitors such as valproic acid can impair oxidative phosphorylation, cytoskeleton remodeling, cell cycle, angiogenesis and ubiquitin-proteasome pathways.[10,11] Treatment with vorinostat, which inhibits Class I, II and IV HDACs can impair the in vitro invasive potential of murine osteosarcoma cell lines.[12] Further, osteosarcoma cell lines are highly sensitive to panobinostat treatment at nanomolar concentrations.[6] Here we report, using in vivo models of osteosarcoma, that panobinostat as a single agent is highly effective at preventing orthotopic osteosarcoma growth, spontaneous lung metastasis, lung colonization by osteosarcoma cell lines and the outgrowth of established osteosarcoma lung metastases. Additionally, genetic and pharmacological studies establish key roles of HDAC1 and HDAC2 in controlling the progression of the disease.

2 MATERIALS AND METHODS

2.1 Cell lines and cell culture

K7M2 (RRID: CVCL_V455; a kind gift from Dr Chand Khanna, NCI[13]), SAOS2 (RRID:CVCL_0548) and SAOS2-LM7 (RRID:CVCL_0515; a kind gift from Dr Eugenie Kleinerman, MD Anderson,[14]), and primary murine mesenchymal stromal cells (MSCs) were isolated from the cortical bone of C57BL/6 mice. All cell lines were mycoplasma free (Cat # CUL001B, R&D Systems, Minneapolis, Minnesota). All human cell lines were validated by short tandem repeat (STR Moffitt genomics core) and mouse cell lines via IDEXX BioAnalytics within the last 6 months. Cell lines were passaged in the recommended culture medium supplemented with 10% fetal calf serum. All cell lines were transduced to express luciferase using Cignal Lenti Positive Control (luc; Qiagen CAT# 336891). Positive clones were selected using puromycin.

2.2 HDAC qRT-PCR, immunoblotting and silencing

Total RNA was extracted from cells with TRIzol (Invitrogen, Carlsbad, he California)as per manufacturer's instructions. HDAC human and mouse primers were synthesized (IDT) (Table S1). RT-PCR mixtures were generated using SYBR Green reagent (Applied Biosystems, Foster City, California, Cat#: 4309155) and reactions were performed and quantified using ABI-7900HT instrument and SDS 2.3 software as per manufacturer's instructions (Applied Biosystems).

For analysis of protein levels by immunoblotting, cells were lysed with RIPA (150 mM NaCl, 1 mM EDTA, 1% Triton X-100, 1% sodium deoxycholate, 0.1% SDS, 20 mM Tris, pH 8). Protein concentration was determined by BCA (Pierce, Waltham, Massachusetts, #23225). Blots were blocked in 5% BSA for 1 hour followed by primary antibody. Primary antibodies for HDAC1, HDAC2, HDAC3 and HDAC5 were purchased from Cell Signaling (Cat # 2062, 57156, 85057 and 20458). HDAC6 antibody was purchased from Abclonal (Cat # A11259). HDAC8 and HDAC11 antibodies were a kind gift from Dr Ed Seto (George Washington University). All primary antibodies were diluted 1:1000 in blocking solution +0.1% Tween-20, and incubated overnight at 4°C. Actin (Santa Cruz sc-1615 or Cell Signaling Technology, Danvers, Massachusetts, #3700) was used as a loading control. Blots were washed, then incubated with HRP-conjugated antispecies secondary (Cell Signaling Technology, Rabbit #7074/Mouse #7076, 1:1000) and developed by enhanced chemiluminescence followed by exposure to light-sensitive film or imaging by LI-COR Odyssey Fc. Quantification performed w Image Studio software (LI-COR).

For HDAC1, HDAC2 and HDAC5 silencing, siRNA was purchased from Santa Cruz Biotechnology (Dallas, Texas, Cat # sc-29344, sc29346, sc-35542, control siRNA sc-37007). HDAC6 siRNA was purchased from Dharmacon (Cat # L-043456–02-005). siRNA transfections were performed using Lipofectamine RNAiMAX Cat # 13778030) according to manufacturer's instructions.

2.3 Cytotoxicity assays

SAOS2, SAOS2 LM7 and K7M2 cells were seeded 5×10^3 cells per well in 96-well plates and in triplicate were treated with a dose range of panobinostat (Selleckchem, Houston, Texas, Cat #S1030; 1.8, 2.4, 3.3, 4.5, 6.0, 8.1, 11.0, 14.8 and 20 nM) or a dose range of romidepsin (Selleckchem Cat #S3020; 5.9, 8.8 13.2, 19.8, 29.6, 44.4, 66.7, 100 and 150 nM). For dual treatment with Panobinostat and Carfilzomib (Selleck Cat #S2853) K7M2 and SAOS2 cells were plated at 5×10^3 cells in 96-well plates and treated with panobinostat at a dose range (1.4, 1.8, 2.5, 3.3, 4.5, 6.1, 8.2, 11.1 and 15 nM) or carfilzomib at a dose range (1.9, 2.6, 3.5, 4.7, 6.3, 8.5, 11.5, 15.6 and 21 nM) or combination of both drugs. IC_{50} values were determined at 48 hours posttreatment using cell titer blue assay (Promega, Madison, Wisconsin, Cat # G8080). To determine the tubastatin (Selleckchem Cat # S2627), IC_{50} value K7M2 cells were seeded at 2×10^4 in 96-well plates and treated with the following concentrations (0, 1, 5, 10, 15, 100, 250, 500, 1250, 2500, 5000 and 10 000 nM). All treatments were done in triplicate and cell growth was assayed at 48 hours using MTS CellTiter 96 cell proliferation assay (Promega Cat # G5421). The impact of panobinostat and romidepsin on PDX derived cell lines was examined in a publicly available dataset (https://braid.stjude.org/masttour/).[15]

2.4 In vivo studies

All in vivo studies were performed under the Moffitt/University of South Florida Institute of Animal Care and Use Committee approved protocol R3540 (CCL). For in vivo experiments K7M2 or SAOS2-LM7 luciferase-expressing cells were injected into BalB/c or NSG mice, respectively. For the primary osteosarcoma study 1×10^5 cells were injected intratibially in 20 μL of sterile PBS into one of the hind tibias. The other hind tibia was injected with 20 μL of sterile PBS as a control. For the lung seeding studies, 1×10^6 K7M2 cells were injected intravenously by tail vein injection. For treatment with panobinostat (10 mg/kg in 10 mM Citrate buffer with 10% Captisol (Cydex Pharmaceuticals, San Diego, California, Cat # Rc-OC7–100) mice were randomized into cohorts for treatment by intraperitoneal injections in 200 μL volumes of either panobinostat or vehicle for the remainder of the study (5 days on, 2 days off treatment). Treatments with romidepsin 2.4 mg/kg dissolved in 2% DMSO, 30% 400PEG, 5% Tween 80 in ddH20 were administered twice a week subcutaneously in 100 μL volumes. Treatment with Carfilzomib (2 mg/kg in 10 mM Citrate buffer with 10% Captisol) was administered by tail vein injection in 100 μL volumes on two consecutive days followed by 5 days no treatment. In the dual panobinostat carfilzomib treated mice group, we treated with one-tenth of the dose of the individual drugs (0.2 mg/kg carfilzomib and 1 mg/kg panobinostat). Each week, mice received both carfilzomib and panobinostat on Days 1 and 2 followed by 3 days of panobinostat only and then 2 days no treatment. Bioluminescence for all studies was measured as a correlate of tumor growth (IVIS, Perkin Elmer, Waltham, Massachusetts).

2.5 Ex vivo bone analysis

Tibias were collected and fixed in 10% formalin for 24 to 48 hours then transferred to 50% ethanol. Radiographic images (Faxitron, X-ray Corp, Tucson, Arizona) were obtained using energy of 35 kV p and an exposure time of 8 milliseconds. The spatial resolution is 10

lp/mm (48 μm). The tumor volume (TuV) was calculated as a function of the total tissue volume (TV) of the tibial medullary canal using ImageJ software. For μCT analysis, the proximal tibia metaphyses were scanned (μCT-40; Scanco Medical, Wangen-Brüttisellen, Switzerland). An evaluation of trabecular bone structural parameters was performed in a region that consisted of 1 mm starting at 500 μm from the growth plate. A three-dimensional cubical voxel model of bone was built and calculations were made for relative bone volume per total volume and trabecular number. After X-ray and μCT analysis, tibias were decalcified (14% EDTA, pH 7.4, 3 weeks), processed and paraffin-embedded.

2.6 Ex vivo lung analysis

Lungs were inflated with Bouin's fixative and stored in 10% formalin for 24 hours and then transferred to 50% ethanol. One lobe of each lung was paraffin-embedded. Then, 5 μM sections were cut and transferred to slides for H&E staining and microscopy.

2.7 Immunofluorescence

For paraffin-embedded tissues, slides were dewaxed and rehydrated to water. Antigen retrieval was performed by heat (1× Tris EDTA pH 9.0 in pressure cooker, 5 minutes). Slides were blocked in 10% goat serum in 1× TBS for 1 hour at room temperature. Primary antibodies Phospho-Histone H3, Cell Signaling Cat #9701L, 1:400 dilution; Cleaved Caspase 3 1:200 dilution, Cell Signaling Cat #9661S, were diluted in 10% normal goat serum (Vector Laboratories, Burlingame, California, Cat # S-1000) and incubated overnight at 4°C in a humidified chamber. After three washes in 1× TBST followed by one wash in 1× TBS, secondary antibodies (Alexa Fluor Goat Anti Rabbit 568, Thermo Fisher Scientific, Waltham, Massachusetts, #A-11011); Alexa Fluor Goat Anti Mouse 488 (Thermo Fisher Scientific #A32723) were incubated at a 1:1000 dilution in 10% normal goat serum for 1 hour at room temperature. Slides were washed three times in 1× TBS and mounted using Vectashield Antifade Mounting Medium with DAPI (Vector Laboratories, # H-1200). Slides stored under light-proof conditions until image acquisition.

For in vitro immunofluorescent analyses, cells were seeded into eight-well chamber slides (LAB-TEK #154534) at 2×10^4 and cultured overnight before treatment with either 50% MSC CM or DMEM 5% FBS or 100 nM etoposide for 5 hours. Cells were then rinsed with PBS and fixed in 4% PFA at room temperature for 20 minutes. Fixed cells were then blocked for 30 minutes at room temperature in antibody diluting buffer (2% BSA, 0.1% Triton X-100 in PBS). Primary antibodies (Acetyl-Histone H3, Millipore #06–599, 1:400 dilution in antibody diluting buffer; Rabbit IgG Isotype Control, Thermo Scientific #31235) were incubated at room temperature for 30 minutes. Cells were then washed 3× in PBS and incubated with secondary antibody (Alexa Fluor Goat Anti-Rabbit 488, Invitrogen #A-11034, 1:1000 dilution in antibody diluting buffer) for 30 minutes at room temp in the dark. After washing 3× in PBS, culture chambers were removed and the slides mounted with Vectashield Antifade Mounting Medium with DAPI (Vector Laboratories, # H-1200). Mounted slides were stored under light-proof conditions at 4°C until microscopic analysis. For quantitation of immunofluorescent stained samples, three representative images were acquired at 40× magnification and the ratio of positively stained cells to total number of cells per field (using DAPI) were calculated using ImageJ.

2.8 Statistical analysis

To determine statistical significance among groups, t-test or analysis of variance (ANOVA) followed by Tukey's multiple comparison test was performed. A *P*-value <.05 was considered as statistically significant. Data are presented as SE from the mean (SEM). All statistical analyses were performed with Graph Pad Prism 6.0 (GrapPad Inc., La Jolla, California).

3 RESULTS

3.1 Panobinostat prevents the growth of orthotopic osteosarcoma

We initially assessed the activity of panobinostat in three in vivo models of osteosarcoma; murine K7M2,[13] and human SAOS2 and lung metastatic derived SAOS2-LM7 osteosarcoma cell lines[14] that can be orthotopically or tail vein inoculated as models of primary and metastatic disease. qRT-PCR and immunoblot results revealed that several HDACs were expressed in these osteosarcoma cell lines (Figure 1A and Figure S1A). Analysis of the St. Jude PeCan database also revealed the expression of several HDACs in human osteosarcoma patients (n = 107; Figure S1B).[16] In vitro, dose-response studies on osteosarcoma cell lines established that panobinostat had a similar IC_{50} (14.3 nM) in K7M2, SAOS2 (11.98 nM) and SAOS2-LM7 (25 nM; Figure 1B). As expected, panobinostat treatment of all three cell led to increased levels of in acetylated histone H3 (Figure 1C).

To initially test the efficacy of panobinostat in vivo, we utilized the syngeneic K7M2 murine osteosarcoma transplant model in immunocompetent Balb/c mice.[13] Mice were intratibially injected with luciferase-expressing K7M2 cells and contralateral limbs received control injections of saline. Using bioluminescence as a correlate for tumor growth, mice were randomized into vehicle control (*VEH*: n = 11) or panobinostat (*PANO*: n = 11) groups. Panobinostat treatment inhibited or significantly delayed primary osteosarcoma growth (Figure 1D), where analysis of the average bioluminescence reveals significant differences between the groups from Day 14 onwards (Figure 1E). Of note, panobinostat treated mice were given a drug holiday between Days 23 and 30 due to diarrhea and anemia that mitigated the observed toxicities but resulted in osteosarcoma growth. However, upon resuming panobinostat treatment, the disease burden again plateaued. Using a bioluminescence value of 1×10^6 as the study endpoint, the median progression time of 21 days for the control cohort was significantly shorter than the 53 days median for the panobinostat-treated cohort. Treatment was halted on Day 56 and, at that time point, only 54% of the panobinostat-treated mice (n = 6/11) had reached an RLU of 1×10^6 (Figure 1F). Upon reaching endpoint, ex vivo X-ray analysis revealed a significant increase in osteosarcoma induced osteolysis in the vehicle control vs the panobinostat treated cohort (Figure 1G). This was reflected in greater trabecular bone volumes as measured by high-resolution μCT scan analysis although statistical significance was not reached (Figure 1H). Histomorphometry and histological analyses also revealed no striking differences between the groups (data not shown). However, in keeping with bioluminescence data, we observed that panobinostat significantly reduced tumor proliferation and enhanced apoptosis indices as measured by phospho-histone H3 (pHH3) and cleaved caspase 3 (CC3), respectively (Figure 1I,J).

3.2 Panobinostat treatment impairs spontaneous lung metastasis

The K7M2 model spontaneously metastasizes to the lung from the orthotopic site at high frequency.[13] In the vehicle cohort, we observed the median time to detectable lung metastasis, assessed by the appearance of bioluminescent signal, was 10 days vs 21 days for the panobinostat treated mice (Figure 2A). Of note, 27% of the panobinostat treated cohort (n = 3/11) had no evidence of lung metastasis at the study endpoint (Day 56). Further, lung metastases that did form in panobinostat treated recipient mice were significantly smaller than those manifest in the vehicle group (Figure 2B). In accord with this observation, the number of tumor nodules in hematoxylin and eosin (H&E) stained sections were significantly reduced in tumor-bearing lungs obtained from panobinostat treated vs vehicle-treated mice (Figure 2C). The proliferative indices, as measured by pHH3, were also significantly lower in the panobinostat treated cohort while conversely, apoptotic indices (CC3) were significantly higher compared to vehicle control (Figure 2D,E). Thus, panobinostat is a potent inhibitor of primary osteosarcoma growth and metastasis in this aggressive in vivo immunocompetent model of the disease.

3.3 Pretreatment with panobinostat compromises osteosarcoma lung seeding

Given that panobinostat treatment reduced spontaneous osteosarcoma lung metastasis, we next tested if panobinostat would prevent the distant seeding and establishment of osteosarcoma using a tail vein pulmonary metastasis model. The rationale for this in vivo experiment would determine whether panobinostat would potentially be effective clinically as a neoadjuvant or adjuvant therapy postprimary tumor resection in preventing the seeding of lung with osteosarcoma metastases. Mice were divided into vehicle (*VEH*: n = 9) or panobinostat (*PANO*: n = 5) cohorts and treated for 5 days prior to the tail vein inoculation with K7M2 luciferase-expressing cells. Bioluminescent analysis revealed an initial drop in both groups after inoculation but subsequent to engraftment, lower tumor burden and growth rates were observed in the lungs of the panobinostat treated mice (Figure 3A). Analysis of the average bioluminescence revealed significant differences between the groups from Day 27 onwards (Figure 3B). Panobinostat treatment was halted at Day 38 post tumor inoculation as statistical significance had been reached. Progression, using the clinical endpoint of labored breathing or weight loss was then monitored in the remaining mice through Day 92. At Day 74, all control mice had succumbed to lung metastasis with a median survival time of 54 days (Figure 3C). In contrast, only 60% (n = 3/5) of the mice treated with panobinostat for 38 days had succumbed at the study endpoint and the median survival time was significantly higher at 92 days vs the vehicle cohort.

Detailed analyses of lung metastases performed revealed far fewer gross surface metastases in the panobinostat treated group (Figure 3D) as well as reduced numbers of micrometastases (Figure 3E). The metastases were distinct and regardless of group, did not display striking differences in morphology or location within the lung tissues. Interestingly, despite ceasing panobinostat treatment at day 38, proliferative (pHH3) and apoptotic (CC3) indices remained significantly lower and higher, respectively, in the panobinostat treated cohort at the study endpoint (Figure 3F,G). Thus, panobinostat treatment is effective at limiting the colonization of the lung by osteosarcoma cells.

3.4 Panobinostat treatment reduces established osteosarcoma lung metastatic burden

In pretreatment seeding studies, 40% (n = 2/5) of the panobinostat treated mice had detectable tumor burden but remained viable at the study endpoint (Day 97) despite ceasing treatment at day 38. To assess if the outgrowing established metastases remained sensitive to panobinostat, a single mouse from this cohort was retreated with panobinostat on Day 90. Within 1 week, the tumor volume, as measured by bioluminescence, was reduced by approximately 75% (Figure S2). Further, K7M2 metastatic cells isolated from the lungs of panobinostat treated mice, which were selected in culture using puromycin (selection marker for luciferase-expressing cells) containing media, remained sensitive to low nM doses of panobinostat (Figure S2). Thus, these osteosarcoma cell lines did not acquire resistance to the HDAC inhibitor in vivo.

Given that panobinostat impaired osteosarcoma lung seeding, we next tested if this drug would also compromise the growth of established lung metastases. K7M2 cells were tail vein inoculated and allowed to establish and grow in the lung. At day three postinoculation, mice were randomized based on bioluminescence into vehicle control (*VEH*: n = 12) or panobinostat (*PANO*: n = 12) cohorts. Within 72 hours of treatment, a significantly lower growth rate was detected in the panobinostat treated group compared to vehicle control and this difference persisted throughout the remainder of the study (Figure 4A). Analysis of average bioluminescence revealed significant differences between the cohorts from Day 13 onwards (Figure 4B). Using a clinical endpoint of 1×10^6 RLU, overall survival was significantly reduced in the vehicle control group (17 days) compared mice treated with panobinostat (44 days; Figure 4C). Importantly, while all vehicle-treated recipients reached the study endpoint by day 33, 75% of the panobinostat group (n = 9/12) were below this cutoff at day 45. Moreover, analysis of gross and micrometastases revealed a significantly lower lung metastatic burden in the panobinostat vs the vehicle cohort (Figure 4D,E). Finally, analysis of proliferative (pHH3) and apoptotic (CC3) indices revealed lower and higher rates, respectively, of osteosarcoma lung metastatic growth in the panobinostat treated mice compared to vehicle control (Figure 4F,G).

Patients with synchronous or metachronous lung metastatic osteosarcoma have a particularly poor prognosis.[17] We therefore, tested the in vivo efficacy of panobinostat in a model of this disease state, the orthotopic SAOS2-LM7 metastasis model.[14] Again, panobinostat treatment (n = 9) significantly reduced the numbers and growth of SAOS2-LM7 lung metastases vs vehicle-treatedthe cohort (n = 8; Figure S3). Collectively, these models establish panobinostat as an effective single-agent treatment for established lung metastatic osteosarcoma.

3.5 HDAC1 and 2 drive osteosarcoma malignancy

qRT-PCR and immunoblot analysis revealed that several HDACs are expressed in the osteosarcoma cell lines models used (Figures 1A and S1A). To identify the major HDACs necessary for osteosarcoma progression and metastasis we silenced individual HDACs using an siRNA approach. Interestingly, silencing of HDAC5 or HDAC6 significantly increased osteosarcoma growth in vitro (Figure S4a–d), and treatment with the HDAC6 selective inhibitor, tubastatin had little impact on osteosarcoma viability with a IC_{50} of only 13.88

μM; that is, nearly 1000-fold less potent than panobinostat (Figure S4e). Conversely, silencing of HDAC1 or HDAC2 impaired osteosarcoma cell growth (Figure 5A,B). Because we noted compensatory expression of HDAC1 upon HDAC2 silencing, we also examined effects of combined HDAC1/2 silencing, which significantly compromised the growth of the osteosarcoma cells (Figure 5B). In accord with these findings, K7M2 and SAOS2-LM7 cells were highly sensitive to the HDAC1/2 selective inhibitor, romidepsin with IC_{50} values of 50 nM and 5 nM that were similar to those noted for panobinostat (Figure 5C,D). As romidepsin inhibits other HDAC family members at higher concentrations,[18,19] we treated HDAC1/2 silenced cells with romidepsin and found no additional effect on osteosarcoma growth demonstrating the selectivity for romidepsin against HDAC1/2 at the concentrations used (Figure 5E).

Given that patients succumb to established lung metastatic osteosarcoma, we examined the efficacy of romidepsin in treating this stage of the disease. To this end, mice were tail vein inoculated with luciferase-expressing K7M2 and, after 3 days, randomized into vehicle (*VEH*: n = 10) or romidepsin treatment cohorts (*ROMI*: n = 10). Similarly to panobinostat, romidepsin reduced lung metastatic growth as measured by bioluminescence (Figure 6A) and improved overall survival compared to the vehicle cohort (Figure 6B). Again, reduced growth was associated in lower numbers of gross and micrometastases in romidepsin treated mice and an accompanying reduction in proliferation and increased apoptotic indices (Figure 6C–F). We also observed that romidepsin treatment effectively reduces the growth and number of SAOS2-LM7 lung metastases compared to vehicle (n = 8; Figure S3c–e). Based on these data we conclude HDAC1 and 2 contribute to osteosarcoma progression and metastasis.

3.6 Osteosarcoma PDX cell lines are sensitive to romidepsin and/or panobinostat

To determine the robustness of our findings, we examined the sensitivity of patient-derived xenograft (PDX) cell lines in a publicly available dataset (https://braid.stjude.org/masttour/).[15,20] In keeping with our own current and previous data, analyses reveal a broad sensitivity to romidepsin and/or panobinostat in PDX (n = 8) cell lines (Figure 6G).[6,15,20] Interestingly, these studies also documented the synergistic effects of HDAC and proteasome inhibitors in vitro. However, in vivo treatment of PDX models with panobinostat and the proteasome inhibitor, bortezomib, did not prove effective compared to controls.[15] Our previous in vitro studies and analysis of K7M2, SAOS-LM7 also documented the synergy between panobinostat and the proteasome inhibitor, carfilzomib (Figure S5).[6] We next examined the effect of each reagent alone or in combination (at one-tenth of the dose of each single agent based on in vitro data) on the orthotopic growth and spontaneous metastasis of K7M2 in vivo. In contrast to our in vitro data, we observed that, as a single agent, carfilzomib has no effect on primary osteosarcoma growth and ultimately mitigated the beneficial effects observed with panobinostat when given in combination (Figure S5). These data were consistent with previous in vivo studies examining the efficacy of panobinostat and bortezomib in PDX xenografts.[15] Further, carfilzomib alone had no beneficial effect on spontaneous lung metastasis but did not subtract from the efficacy of panobinostat when used in combination. These data underscore the need for in vivo testing of potentially

synergistic therapies identified in vitro but again support the use of HDAC inhibitors for the treatment of primary and metastatic osteosarcoma.

4 DISCUSSION

Although rare, osteosarcoma remains a deadly tumor type, especially for patients with metastatic disease. Despite therapeutic advances for several solid malignancies, the treatment paradigm for osteosarcoma has remained frustratingly static for three decades. Specifically, the 5-year event-free survival rate for osteosarcoma with no metastasis is 60% but this drops to 28% if there is evidence of synchronous metastases.[4] Further, a retrospective analysis of 247 cases of osteosarcoma showed that 13% of patients present with synchronous lung metastases while a further 21% will have metachronous lung involvement within 10 months,[17] and these are responsible for the majority of osteosarcoma related deaths.

Clinical trials of Food and Drug Administration (FDA) therapies for osteosarcoma treatment are difficult and time consuming to conduct given the relative low incidence of disease. To identify effective therapies that will motivate clinical trials, we previously assessed the response of five osteosarcoma cell lines 143B, MNNG/HOS, MG63, U2OS and SAOS2 to a panel of approved therapeutics.[6] We consistently observed that the HDAC inhibitor panobinostat compromised the survival of all osteosarcoma cell lines at low concentrations. These observations are consistent with studies examining the in vitro effects of panobinostat and other broad-spectrum HDAC inhibitors such as vorinostat on osteosarcoma cell lines.[12,21] Independent studies conducting an in vitro screen of drug efficacy on three osteosarcoma PDXs also identified HDAC inhibitors and specifically panobinostat as effective at inducing osteosarcoma cell death.[20] Importantly, panobinostat was noted to have additive cytotoxicity in vitro with chemotherapies commonly used to treat osteosarcoma, doxorubicin and gemcitabine.[20] Collectively, these in vitro studies underscore the potential for HDAC inhibition for the treatment of osteosarcoma.

To date, no studies have assessed the efficacy of panobinostat as a single agent on osteosarcoma in vivo. Here, using several complementary models of human and murine osteosarcoma, we show that panobinostat treatment effectively limits the growth of primary disease and spontaneous metastasis to the lung, and that it can also prevent seeding of the lung tissues by osteosarcoma cells. These data (Figure 3) suggest that applying panobinostat in a neoadjuvant or adjuvant setting for the treatment of primary disease could greatly reduce the incidence of, or time to, metachronous events. Importantly, we also showed that panobinostat significantly reduced the growth of established osteosarcoma lung metastases and greatly extended overall survival. Panobinostat does have noted toxicities such as anemia and diarrhea at the doses and frequency used but mice quickly rebounded during the drug “holiday.” Given the significance of our results, it is likely that panobinostat treatment with lower doses or at longer intervals would remain efficacious. Collectively, these data provide strong rationale for the design of clinical trials to test panobinostat in canine osteosarcoma and ultimately humans. We would anticipate that patients diagnosed with lung metastatic osteosarcoma, that are at most risk and have failed other treatments, would be the focus cohort for such trials.

While presumably, the effects of panobinostat are cancer cell intrinsic, there are also potential benefits on the tumor microenvironment. For example, panobinostat has been shown to prevent osteoclast formation and function.[22] Additionally, in other malignancies, HDAC inhibition in combination with HER2 blocking antibodies has been shown to activate immune cells such as natural killer (NK) cells to improve the tumoricidal effects on HER2 positive breast tumors.[23] In melanoma, panobinostat has been shown to not only inhibit the disease but to also augment the expression of major histocompatibility complex and costimulatory molecules in tumor cells leading to the activation of antigen-specific T-cells.[24] In support of this, the effects of panobinostat and romidepsin in our study were more striking in the syngeneic K7M2 immunocompetent model compared to the SAOS-LM7 immunocompromised model and we will be exploring this further as we develop our studies.

Using siRNA studies guided by the expression of HDACs, the combined functions of HDAC1 and HDAC2 were revealed to contribute to the maintenance of osteosarcoma. Interestingly, silencing of HDAC6 promoted tumor growth but this effect was not observed with the HDAC6 inhibitor tubistatin suggesting potentially noncatalytic tumor-suppressive roles. Notably, analysis of public datasets reveals high expression of HDAC1 in PDX models of osteosarcoma compared to HDAC2 and other HDAC members.[25] Further, consistent with their roles in osteosarcoma cell fate, HDAC1 and HDAC2 are expressed in more mesenchymal/osteoblast precursor states, and their inhibition or deletion promotes osteoblastic differentiation.[26] Finally, although HDAC2 depletion has been reported to promote the stemness of osteosarcoma MG63 cells and in vivo data indicates a tumor-suppressive role for HDAC2,[27] these studies did not assess if there are compensatory effects on *HDAC1* expression.

The key targets being regulated by HDAC1 and HDAC2 that contribute to the maintenance of osteosarcoma levels remain to be elucidated but their identification could lead to the development of more specific targeted therapies for osteosarcoma treatment. Regardless, our studies provide a strong rationale for clinical trials that assess the efficacy of panobinostat or romidepsin for the treatment of metastatic osteosarcoma. To date, no trials with HDAC inhibitors have been conducted for osteosarcoma and we submit these trials should be a high priority, especially given the dearth of effective therapies for metastatic metachronous osteosarcoma, and the fact that both panobinostat and romidepsin are FDA approved for the treatment of other malignancies.

Supplementary Material

Refer to Web version on PubMed Central for supplementary material.

ACKNOWLEDGEMENTS

Authors would like to thank Dr John L. Cleveland at the Moffitt Cancer Center for critical review of this work. The authors thank the Chotiner Foundation (CCL), the National Pediatric Cancer Foundation (DR) and the Moffitt Cancer Center for financial support. This work has been supported in part by the Tissue Core Facility at the H. Lee Moffitt Cancer Center & Research Institute, an NCI designated Comprehensive Cancer Center (P30-CA076292). We would also like to thank Chris Cubitt of the Moffitt Translational Research Core for assistance with IC_{50} determinations and gratefully acknowledge Dr Elizabeth Stewart, St Jude Children's Research Hospital, Memphis, TN and the Childhood Solid Tumor Network for their sharing of available resources (https://www.stjude.org/research/resources-data/childhoodsolid-tumor-network.html).

Funding information

Chotnier Foundation; Comprehensive Cancer Center, Grant/Award Number: P30-CA076292; H. Lee Moffitt Cancer Center & Research Institute; Moffitt Cancer Center; National Pediatric Cancer Foundation

Abbreviations

CC3	cleaved caspase three
FDA	Food and Drug Administration
H&E	hematoxylin and eosin
HDAC	histone deacetylase
MSC	mesenchymal stromal cell
NK cell	natural killer cell
PANO	panobinostat
pHH3	phospho histone H3
RLU	relative light unit
SAOS2	sarcoma osoteogenic2
SAOS-LM7	sarcoma osteogenic-lung metastasis 7
Sir	sirtuin
VEH	vehicle

REFERENCES

1. McGuire J, Utset-Ward TJ, Reed DR, Lynch CC. Re-calculating! Navigating through the osteosarcoma treatment roadblock. Pharmacol Res. 2017;117:54–64. [PubMed: 27940205]
2. Luetke A, Meyers PA, Lewis I, Juergens H. Osteosarcoma treatment— where do we stand? A state of the art review. Cancer Treat Rev. 2014; 40:523–532. [PubMed: 24345772]
3. Mc Auley G, Jagannathan J, O'Regan K, et al. Extraskeletal osteosarcoma: spectrum of imaging findings. AJR Am J Roentgenol. 2012;198: W31–W37. [PubMed: 22194512]
4. Smeland S, Bielack SS, Whelan J, et al. Survival and prognosis with osteosarcoma: outcomes in more than 2000 patients in the EURAMOS-1 (European and American osteosarcoma study) cohort. Eur J Cancer. 2019;109:36–50. [PubMed: 30685685]
5. Roberts RD, Lizardo MM, Reed DR, et al. Provocative questions in osteosarcoma basic and translational biology: a report from the Children's oncology group. Cancer. 2019;125:3514–3525. [PubMed: 31355930]
6. Yu D, Kahen E, Cubitt CL, et al. Identification of synergistic, clinically achievable, combination therapies for osteosarcoma. Sci Rep. 2015;5:16991. [PubMed: 26601688]
7. Panobinostat approved for multiple myeloma. Cancer Discov 2015; 5: OF4.
8. Li X, Zhang J, Xie Y, Jiang Y, Yingjie Z, Xu W. Progress of HDAC inhibitor panobinostat in the treatment of cancer. Curr Drug Targets. 2014; 15:622–634. [PubMed: 24597570]
9. Li Y, Seto E. HDACs and HDAC inhibitors in cancer development and therapy. Cold Spring Harb Perspect Med. 2016;6:a026831. [PubMed: 27599530]

10. Yamanegi K, Kawabe M, Futani H, et al. Sodium valproate, a histone deacetylase inhibitor, modulates the vascular endothelial growth inhibitor-mediated cell death in human osteosarcoma and vascular endothelial cells. Int J Oncol. 2015;46:1994–2002. [PubMed: 25778932]
11. Wittenburg LA, Ptitsyn AA, Thamm DH. A systems biology approach to identify molecular pathways altered by HDAC inhibition in osteosarcoma. J Cell Biochem. 2012;113:773–783. [PubMed: 21976144]
12. Mu X, Brynien D, Weiss KR. The HDAC inhibitor Vorinostat diminishes the in vitro metastatic behavior of osteosarcoma cells. Biomed Res Int. 2015;2015:290368. [PubMed: 25785263]
13. Khanna C, Prehn J, Yeung C, Caylor J, Tsokos M, Helman L. An orthotopic model of murine osteosarcoma with clonally related variants differing in pulmonary metastatic potential. Clin Exp Metastasis. 2000;18:261–271. [PubMed: 11315100]
14. Jia SF, Worth LL, Kleinerman ES. A nude mouse model of human osteosarcoma lung metastases for evaluating new therapeutic strategies. Clin Exp Metastasis. 1999;17:501–506. [PubMed: 10763916]
15. Stewart E, Federico SM, Chen X, et al. Orthotopic patient-derived xenografts of paediatric solid tumours. Nature. 2017;549:96–100. [PubMed: 28854174]
16. Zhou X, Edmonson MN, Wilkinson MR, et al. Exploring genomic alteration in pediatric cancer using ProteinPaint. Nat Genet. 2016;48:4–6. [PubMed: 26711108]
17. Aljubran AH, Griffin A, Pintilie M, Blackstein M. Osteosarcoma in adolescents and adults: survival analysis with and without lung metastases. Ann Oncol. 2009;20:1136–1141. [PubMed: 19153114]
18. National Center for Biotechnology Information. PubChem Database. Romidepsin, CID=5352062.
19. Falkenberg KJ, Johnstone RW. Histone deacetylases and their inhibitors in cancer, neurological diseases and immune disorders. Nat Rev Drug Discov. 2014;13:673–691. [PubMed: 25131830]
20. Loh AHP, Stewart E, Bradley CL, et al. Combinatorial screening using orthotopic patient derived xenograft-expanded early phase cultures of osteosarcoma identify novel therapeutic drug combinations. Cancer Lett. 2019;442:262–270. [PubMed: 30395907]
21. Wirries A, Jabari S, Jansen EP, et al. Panobinostat mediated cell death: a novel therapeutic approach for osteosarcoma. Oncotarget. 2018;9: 32997–33010. [PubMed: 30250645]
22. Imai Y, Ohta E, Takeda S, et al. Histone deacetylase inhibitor panobinostat induces calcineurin degradation in multiple myeloma. JCI Insight. 2016;1:e85061. [PubMed: 27699258]
23. Medon M, Vidacs E, Vervoort SJ, et al. HDAC inhibitor pan engages host innate immune defenses to promote the tumoricidal effects of trastuzumab in HER2(+) tumors. Cancer Res. 2017;77:2594–2606. [PubMed: 28249907]
24. Woods DM, Woan K, Cheng F, et al. The antimelanoma activity of the histone deacetylase inhibitor panobinostat (LBH589) is mediated by direct tumor cytotoxicity and increased tumor immunogenicity. Melanoma Res. 2013;23:341–348. [PubMed: 23963286]
25. Neale G, Su X, Morton CL, et al. Molecular characterization of the pediatric preclinical testing panel. Clin Cancer Res. 2008;14:4572–4583. [PubMed: 18628472]
26. Lee HW, Suh JH, Kim AY, Lee YS, Park SY, Kim JB. Histone deacetylase 1-mediated histone modification regulates osteoblast differentiation. Mol Endocrinol. 2006;20:2432–2443. [PubMed: 16728531]
27. La Noce M, Paino F, Mele L, et al. HDAC2 depletion promotes osteosarcoma's stemness both in vitro and in vivo: a study on a putative new target for CSCs directed therapy. J Exp Clin Cancer Res. 2018;37:296. [PubMed: 30509303]

What's new?

Clinical trials of osteosarcoma therapies are difficult to conduct given the low incidence of the disease. While in vitro studies have identified histone deacetylase (HDAC) inhibitors as a potential treatment, their efficacy in vivo largely remains untested. This study found that the broad-spectrum HDAC inhibitor panobinostat blocks spontaneous osteosarcoma metastasis to the lung when used as a single agent. Panobinostat also impaired growth of established lung metastases and improved overall survival. Mechanistically, HDAC1/2 emerged as important drivers of osteosarcoma growth and metastasis. Altogether, the findings provide a strong rationale for the design of clinical trials to test panobinostat in humans.

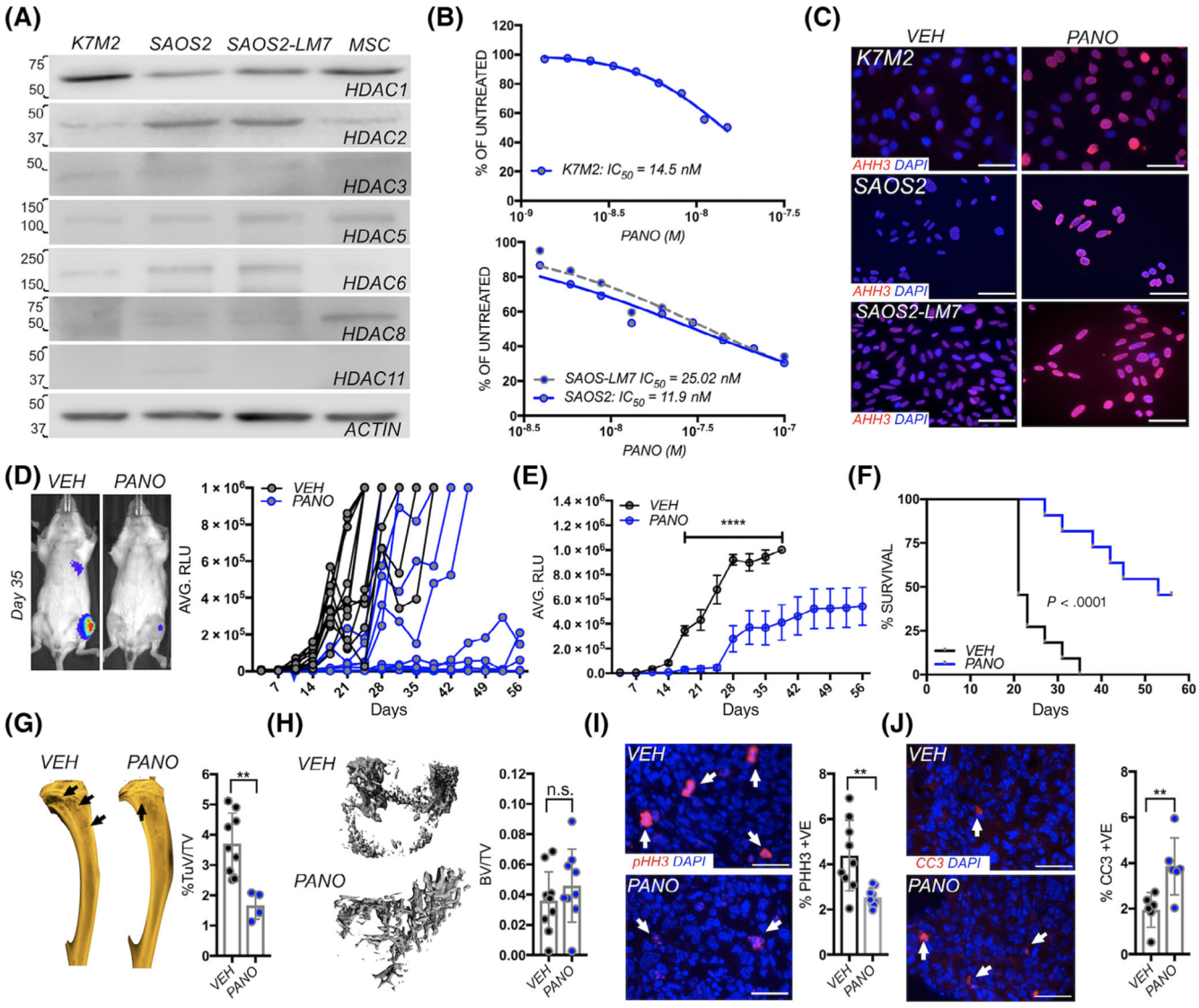

FIGURE 1.

Panobinostat treatment impairs primary osteosarcoma growth and associated bone disease. A, Analysis of HDAC expression in the K7M2, SAOS2 and SAOS2-LM7 osteosarcoma cell lines. Actin (representative image) was used as a loading control. Primary mouse mesenchymal stem cells (MSC) were used as a positive control. Numbers indicate molecular weight (kDa). B, K7M2, SAOS2 and SAOS2-LM7 cell lines were incubated with the indicated concentrations of panobinostat for 24 hours. Cell viability (CellTiter blue) is presented as a percentage of vehicle control. C, Acetylated Histone H3 (AHH3; red) immunofluorescent staining in vehicle control (*VEH*) and panobinostat (*PANO*: 40 nM) treated K7M2, SAOS2 and SAOS2-LM7 cells after 16 hours. DAPI (blue) was used a nuclear stain. D, Spider plot of K7M2 bioluminescence (RLU) over time in individual vehicle control (*VEH*; n = 11) and panobinostat (*PANO*; n = 11) treated mice. Treatment was initiated 3 days subsequent to inoculation (blue arrow). Mice were removed from study upon reaching 1×10^6 relative light units (RLU). Representative images show bioluminescence in each group at Day 35 with hotter colors indicating greater tumor burden.

E, Average of bioluminescence in vehicle control and treated mice. C, Kaplan-Meier curve of time to reach clinical endpoint (RLU = 1×10^6) for orthotopic K7M2 cells in the panobinostat (*PANO*) and vehicle control (*VEH*) groups. F, X-ray analysis of tumor-induced osteolysis (arrow) in vehicle control (*VEH*) and panobinostat (*PANO*) treated groups. Tumor-induced osteolytic area (TuV) was measured as a function of the total volume (TV) of the marrow cavity. G, μCT analysis of trabecular bone volume in vehicle control (*VEH*) and panobinostat (*PANO*) treated groups. Trabecular bone volume (BV) was measured as a function of the total volume (TV) of the marrow cavity. H, I, ex vivo analyses from study endpoint of proliferative and apoptotic indices using phospho-histone H3 (pHH3; red arrows; H) and cleaved caspase 3 (CC3; red, arrows, I), respectively. Scale bars represent 50 μm. Asterisks denote statistical significance (** $P < .01$; n.s. denotes nonsignificance)

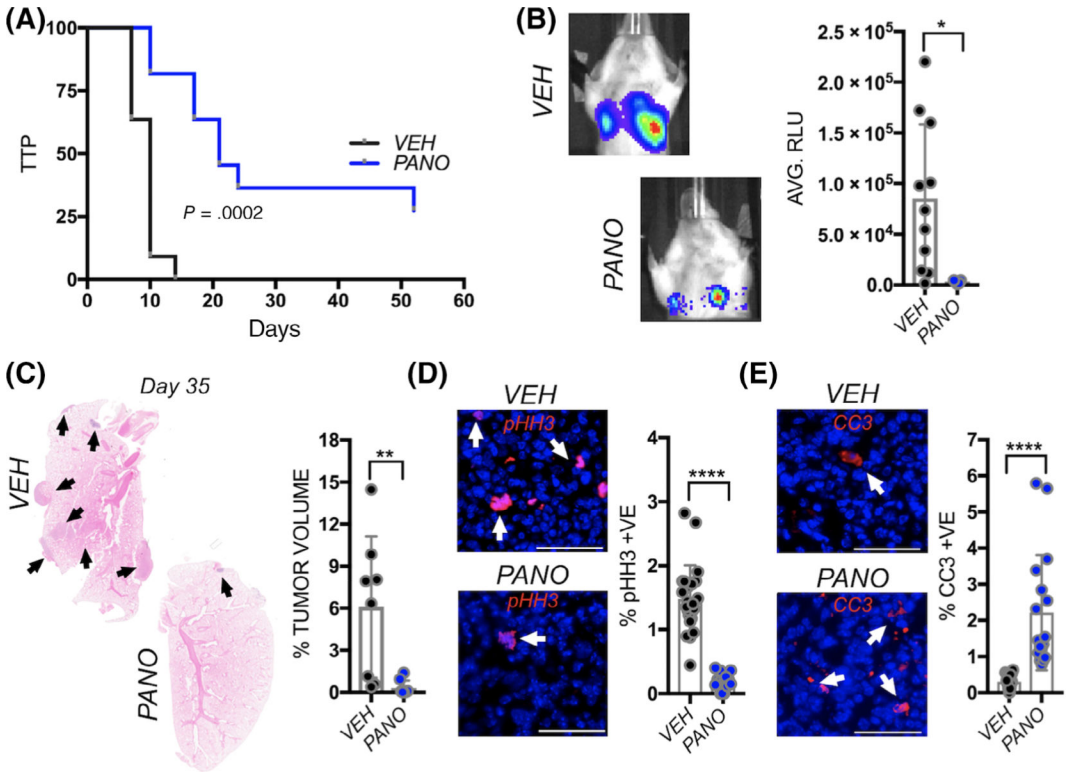

FIGURE 2.

Panobinostat treatment compromises spontaneous osteosarcoma lung metastasis. A, Kaplan-Meier curve of time to progression (TTP) of lung bioluminescence detection in mice bearing primary (tibial) K7M2 tumors in the vehicle control (*VEH*; n = 11/11) group and panobinostat (*PANO*; n = 8/11) treated groups. B, Analysis of bioluminescence (AVG. RLU) in spontaneous metastases arising from orthotopic primary K7M2 tumors in the vehicle control (*VEH*; n = 11/11) group and panobinostat (*PANO*; n = 8/11) treated groups. C, Tumor volume of lung metastases (arrows) as a percentage of total volume in H&E stained sections derived from vehicle control (*VEH*) and panobinostat (*PANO*) treated mice. Arrows indicate metastatic lesions. D, E, ex vivo analyses from study endpoint of proliferative and apoptotic indices using phospho-histone H3 (pHH3; red arrows; D) and cleaved caspase 3 (CC3; red, arrows, E), respectively. Scale bars represent 50 μm. Asterisks denote statistical significance (**P* < .05, ***P* < .01; *****P* < .0001; n.s. denotes nonsignificance)

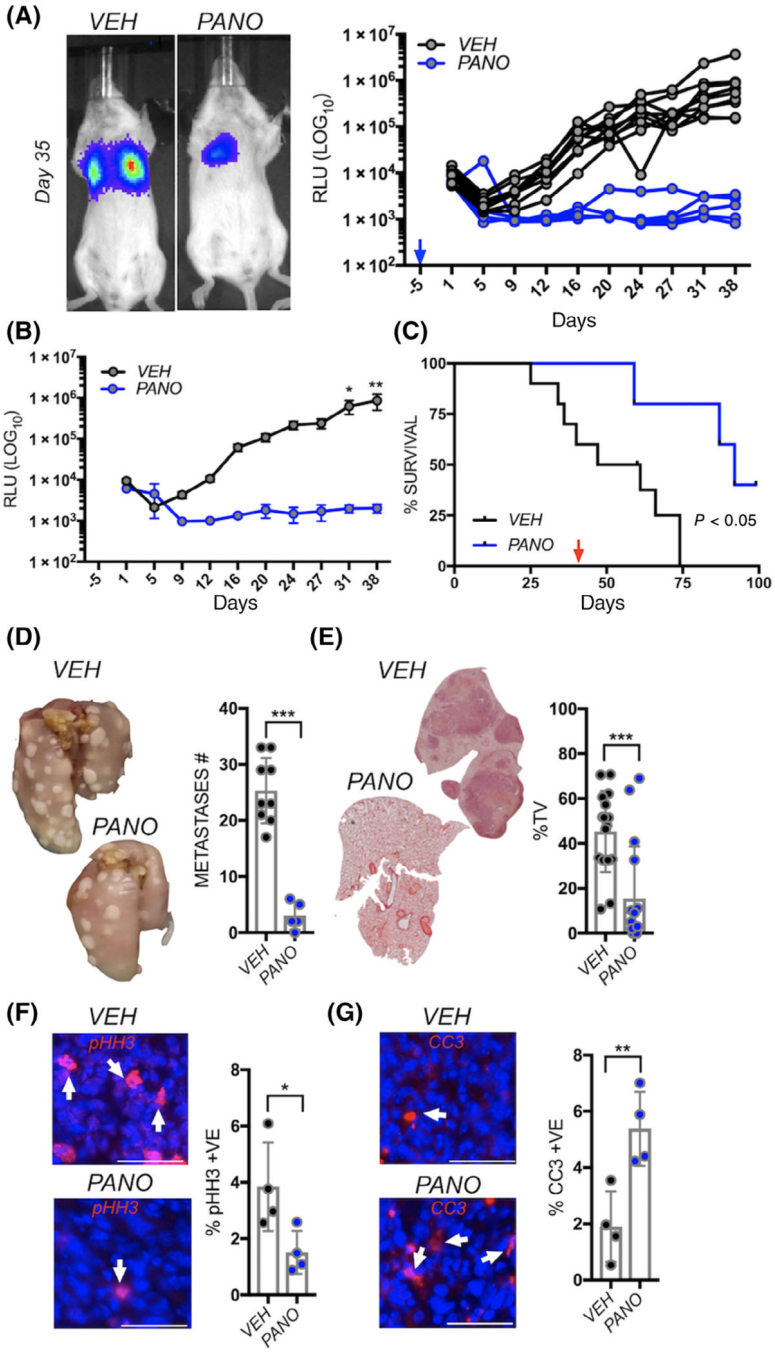

FIGURE 3.

Panobinostat prevents seeding of lung metastatic osteosarcoma. A, Spider plot of K7M2 bioluminescence (RLU) over time in individual pretreated vehicle control (*VEH*; n = 9) and panobinostat (*PANO*; n = 5) treated mice. Treatment was initiated 5 days prior to tail vein inoculation of the osteosarcoma cells (blue arrow). Representative images show bioluminescence in each group at Day 35. B, Average of bioluminescence in vehicle control and treated mice. C, Kaplan-Meier curve of time to reach clinical endpoint in the panobinostat (*PANO*) and vehicle control (*VEH*) groups. Panobinostat treatment was

stopped at Day 38 (red arrow) once statistical significance in overall survival had been reached. At Day 97, all remaining mice in the panobinostat group were euthanatized (n = 2). D, Lungs from each group were inflated with formalin upon removal and the number of surface metastases (Metastases #) counted. E, Lung sections derived from each group were stained with hematoxylin and eosin and the percent tumor volume as a function of total lung volume calculated. F, G, ex vivo analyses from study endpoint of proliferative and apoptotic indices using phospho-histone H3 (pHH3; red arrows; F) and cleaved caspase 3 (CC3; red, arrows, G) respectively. Scale bars represent 50 μm. Asterisks denote statistical significance (*$P < .05$; **$P < .01$; ***$P < .001$)

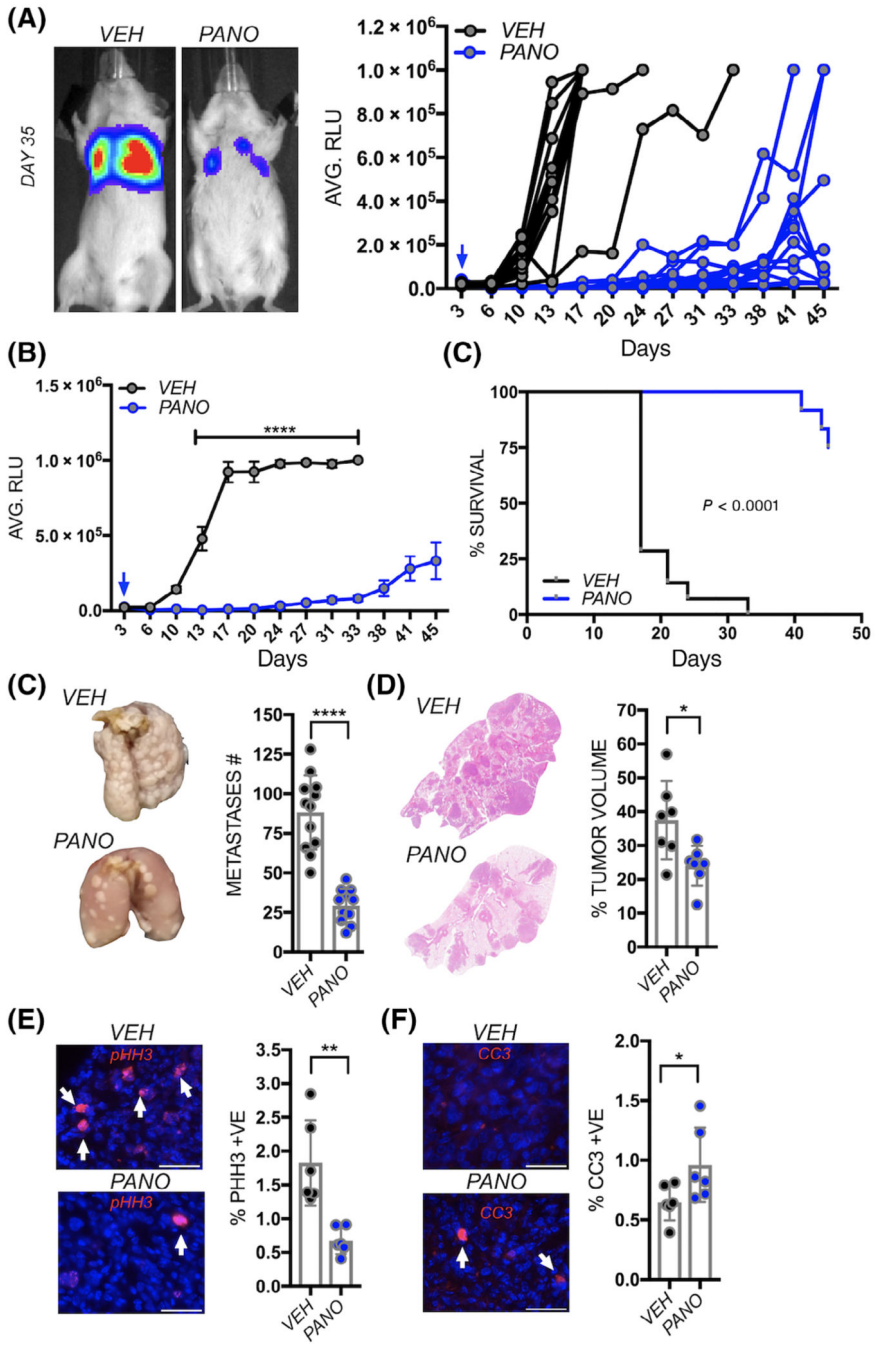

FIGURE 4.

Panobinostat impairs the growth of established lung metastatic osteosarcoma. A, Spider plot of K7M2 bioluminescence over time in individual vehicle control (*VEH*; n = 12) and panobinostat (*PANO*; n = 12) treated mice. Treatment was initiated 3 days postinoculation of the osteosarcoma cells (blue arrow). Representative images show bioluminescence in each group at Day 35. B, Average of bioluminescence in vehicle control and treated mice. C, Kaplan-Meier curve of time to reach clinical endpoint in the panobinostat (*PANO*) and vehicle control (*VEH*) groups. D, Lungs from each group were inflated with formalin upon

removal and the number of surface metastases (Metastases #) counted. E, Lung sections derived from each group were stained with hematoxylin and eosin and the percent tumor volume as a function of total lung volume calculated. F, G, ex vivo analyses from study endpoint of proliferative and apoptotic indices using phospho-histone H3 (pHH3; red arrows; F) and cleaved caspase 3 (CC3; red, arrows, G), respectively. Scale bars represent 50 μm. Asterisks denote statistical significance (*$P < .05$; **$P < .01$; ***$P < .001$)

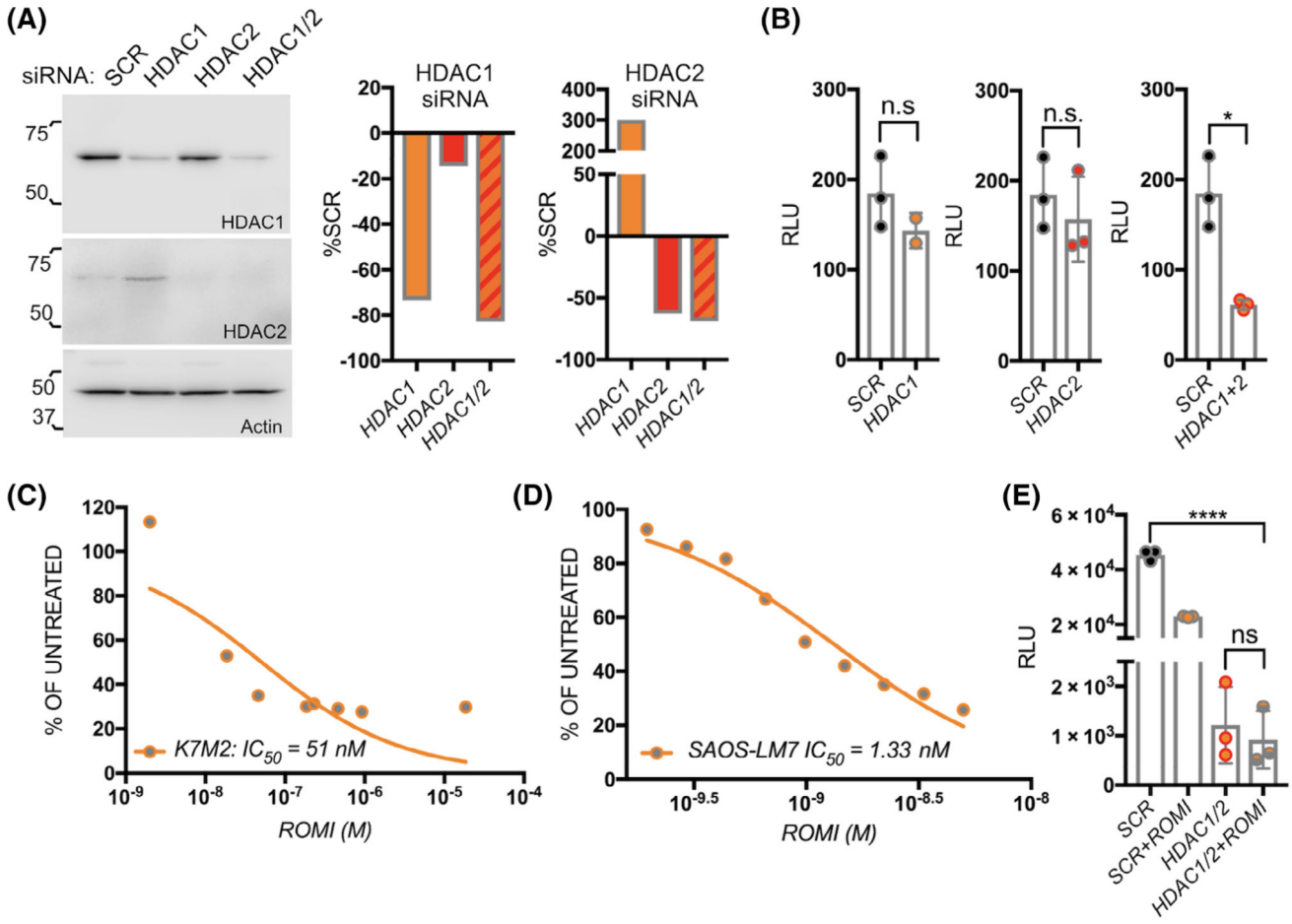

FIGURE 5.

HDAC1 and 2 contribute to osteosarcoma growth. A, B, Analysis of HDAC1 and HDAC2 levels in K7M2 cells 48 hours subsequent to siRNA silencing (A) each HDAC individually or in combination (HDAC1/2) compared to scrambled control siRNA (SCR). Actin was used as a positive loading control. Numbers indicate molecular weight (kDa). Densitometry graphs illustrate the impact on HDAC1 and HDAC 2 levels. The impact on cell growth subsequent to silencing HDAC1 and HDAC2 or HDAC1/2 (B) was determined by measuring bioluminescence (RLU). C, D, The effect of the HDAC1/2 selective inhibitor romidepsin at varying concentrations over 48 hours on K7M2 (C) and SAOS2-LM7 (D) cell viability. E, Romidepsin effects on the viability of HDAC1/2 silenced K7M2 compared to scrambled control (SCR) after 24 hours of treatment. Asterisks denote statistical significance (*$P < .05$; ****$P < .0001$; n.s. denotes nonsignificance)

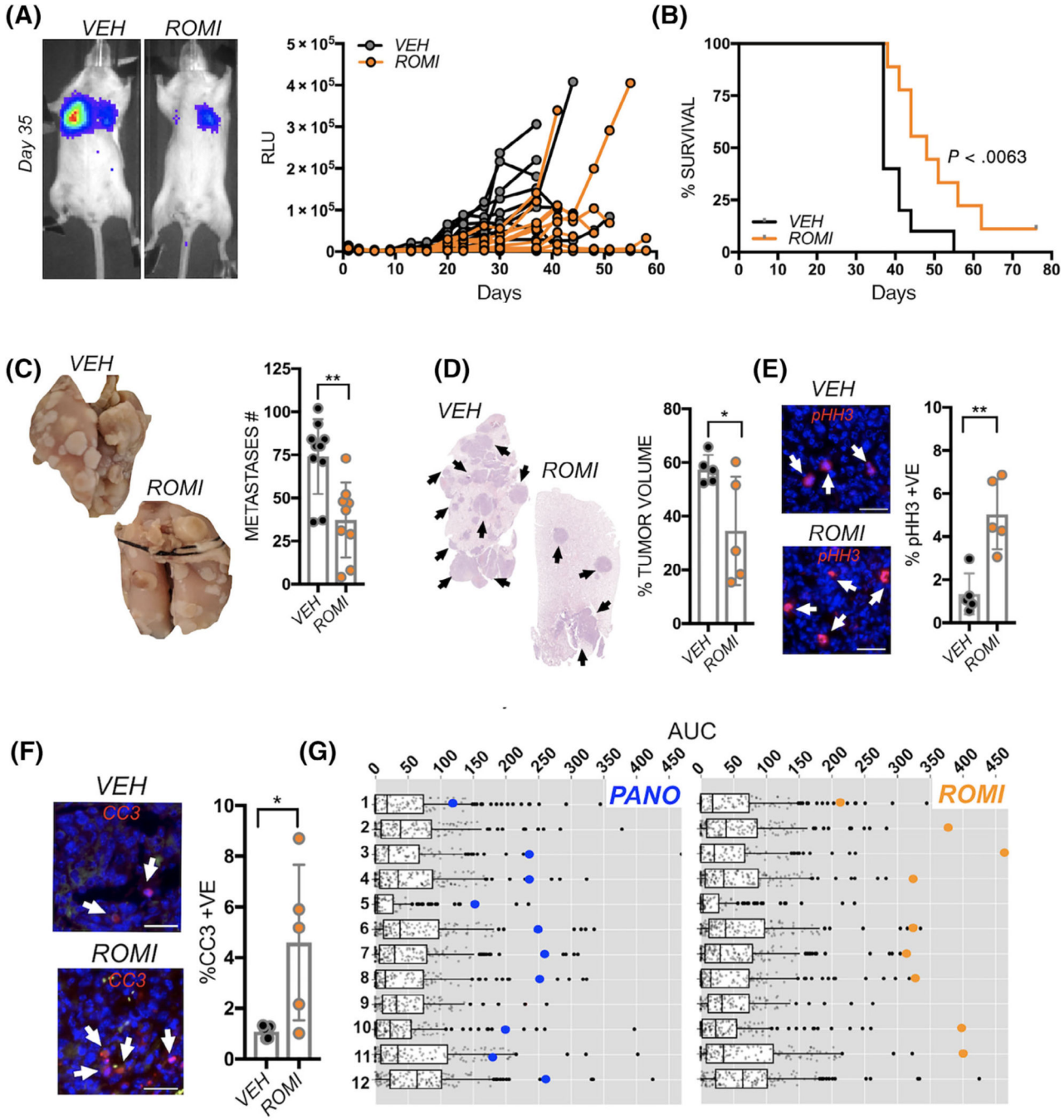

FIGURE 6.

The HDAC1/2 inhibitor romidepsin significantly impacts the growth of established lung metastatic osteosarcoma and the viability of human osteosarcoma PDX cell lines. A, Spider plot of K7M2 bioluminescence over time in individual vehicle control (*VEH*; n = 10) and romidepsin (*ROMI*; n = 10) treated mice. Treatment was initiated 3 days postinoculation of the osteosarcoma cells (blue arrow). Representative images show bioluminescence in each group at Day 35. B, Kaplan-Meier curve of time to reach clinical endpoint in the romidepsin (*ROMI*) and vehicle control (*VEH*) groups. C, Lungs from each group were inflated with

formalin upon removal and the number of surface metastases (Metastases #) counted. D, Lung sections derived from each group were stained with hematoxylin and eosin and the percent tumor volume as a function of total lung volume calculated. E, F, ex vivo analyses from study endpoint of proliferative and apoptotic indices using phospho-histone H3 (pHH3; red arrows; E) and cleaved caspase 3 (CC3; red, arrows, F) respectively. Scale bars represent 50 μm. Asterisks denote statistical significance (*$P < .05$; **$P < .01$; ***$P < .001$). F, Analysis of patient-derived xenograft (PDX; SJOS series) cell line response to panobinostat (*PANO*; blue dots) and romidpesin (*ROMI*; orange dots). (https://braid.stjude.org/masttour/). 1: CY143B, 2: SAOS2, 3: SAOS2-LM7, 4: SJOS001105_X1, 5: SJOS001107_X1, 6: SJOS001107_X2, 7: SJOS001107_X3, 8: SJOS001108_X1, 9: SJOS001112_X1, 10: SJOS010929_X1, 11: SJOS013769_X1 and 12: U20S. AUC represents the area under curve while black dots represent the effectiveness of other reagents